Supplementary Materials

Hierarchical porous Co-rich PtCo thin films for alkaline seawater hydrogen evolution with chlorine corrosion resistance

Meilin Zhang[1], Hanzhong Cui[2, 3], Zhou Yang[2, 3], Jie Yan[2, 3], Jin Zhang[2, 3 *], Huan Ma[2, 3], Renguo Guan[2, 3 **]

[1] School of Materials Science and Engineering, Northeastern University, Shenyang 110819, China;

[2] Key Laboratory of Near-Net Forming of Light Metals of Liaoning Province, Dalian Jiaotong University, Dalian 116028, China

[3] Engineering Research Center of Continuous Extrusion, Ministry of Education, Dalian Jiaotong University, Dalian 116028, China;

[*] Correspondence: jinzhang@djtu.edu.cn (J.Z.)

[**] Co-Correspondence: guanrenguo@sina.cn (R.G.)

Preparation of Pt/C electrode

100 μL Nafion solution (5 wt.%) was diluted with 3 mL isopropanol. The 9 mg commercial 20 wt.% Pt/C was uniformly dispersed into the diluted Nafion solution by ultrasonic treatment. Subsequently, 15 μL of the mixed solution was dropped onto the surface of the pre-polished glassy carbon electrode (GCE, diameter: 5 mm). After natural drying at room temperature, it is used as a working electrode for HER test.

Tafel slope and HER mechanism

The Tafel slopes of catalysts were calculated from the LSV curves, according to formula (S1) [S1, S2]:

$$\eta = a + b \lg j \quad \text{(S1)}$$

where η is overpotential (V vs. RHE), a is the y-axis intercept, b is Tafel slope (mV sec^{-1}), and j is current density (mA cm^{-2}).

The HER mechanism can be interrogated from the Tafel slopes. In alkaline environment, the electrolysis of water includes the following cathodic hydrogen evolution reaction and anodic oxygen evolution reaction [S3]:

Cathode: $2H_2O + 2e^- \rightarrow H_2 + 2OH^-$ (S2)

Anode: $4OH^- \rightarrow O_2 + 2H_2O + 4e^-$ (S3)

The cathodic hydrogen evolution reaction usually includes two steps. The first step is called the Volmer step (120 mV sec^{-1}), in which electrons on the cathode surface attract H_2O molecules from the electrolyte to produce adsorbed H atoms (H*) as reaction intermediates [S4]:

Volmer step: $H_2O + e^- + * \rightarrow H^* + OH^-$ (S4)

The second step involves the formation of H_2 molecules. The coverage of H* on the cathode surface determines two different pathways [S4]:

Heyrovsky step: $H^* + H_2O + e^- \rightarrow H_2 + OH^- + *$ (S5)

Tafel step: $2H^* \rightarrow H_2$ (S6)

where * refers to an active site. When the coverage of H* on the cathode surface is low, H* is easy to combine with additional electrons and a new H_2O molecule to form H_2 molecules, which is called the Heyrovsky step (40 mV sec^{-1}). On the contrary, the high H* coverage makes the second step occur as a Tafel step (30 mV sec^{-1}), in which two adjacent H* bind to form H_2 molecules. Tafel step is a chemical desorption process.

Electrochemical active area (ECSA) and roughness factor (RF)

The charging current ΔI (mA) of catalysts at open circuit potential is calculated according to formula (S7) [S5]:

$$\Delta I = \left| I_{cathode} - I_{anode} \right|_{ocp} \quad \text{(S7)}$$

where $I_{cathode}$ and I_{anode} are cathode current (mA) and anode current (mA) at open circuit potential, respectively.

The double-layer capacitance values C_{dl} (mF) are determined based on formula (S8) [S5]:

$$C_{dl} = \frac{\Delta I}{2\Delta v} \times 1000 \quad \text{(S8)}$$

where Δv is the scan rate in the CV test (mV s^{-1}).

The ECSA (cm^2) of the catalysts is estimated using formula (S9) [S5]:

$$ECSA = \frac{C_{dl}}{C_s} \quad \text{(S9)}$$

Where C_s represents the specific capacitance in alkaline media, the value of which is 0.04 mF cm^{-2}.

The RF of the catalysts can be further calculated through formula (S10) [S5]:

$$RF = \frac{ECSA}{S} \quad \text{(S10)}$$

where *S* is the geometric area of the catalysts with a value of 0.25 cm^{-2}.

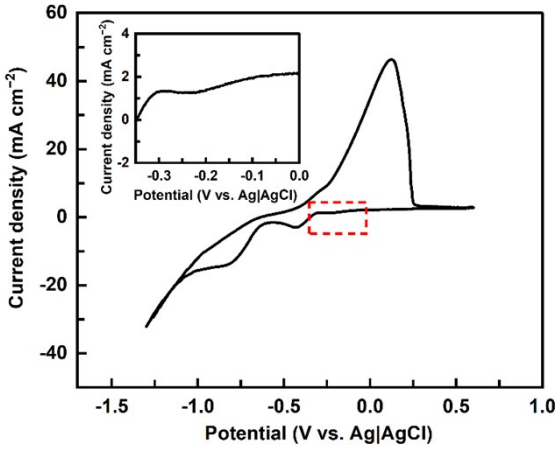

Fig. S1. CV of the electrolyte on a vitreous carbon electrode under stagnant conditions. Electrolyte contains 2 mM Na_2PtCl_6, 200 mM $CoCl_2$, 0.1 M NH_4Cl, 0.2 M H_3BO_3, and 40 g L^{-1} F127.

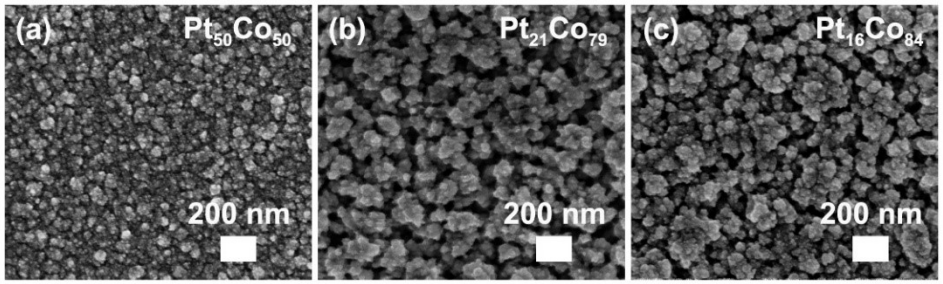

Fig. S2. Magnified SEM image of (a) $Pt_{50}Co_{50}$, (b) $Pt_{21}Co_{79}$, and (c) $Pt_{16}Co_{84}$.

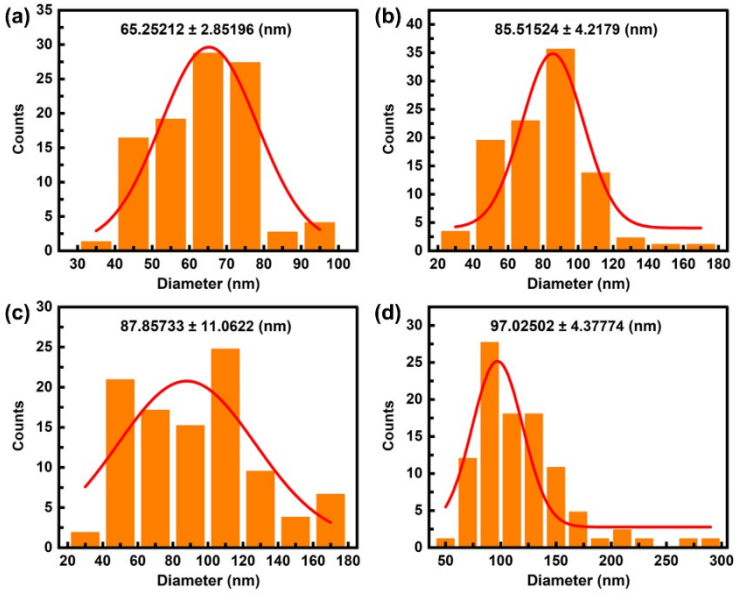

Fig. S3. The particle size distribution statistics of (a) $Pt_{50}Co_{50}$, (b) $Pt_{34}Co_{66}$, (c) $Pt_{21}Co_{79}$, and (d) $Pt_{16}Co_{84}$ depicted in Fig. 1f and Fig. S2.

Table S1. Binding energies for Pt 4f and Co 2p signals of PtCo thin films.

Sample	Binding energy (eV)			
	Pt $4f_{7/2}$	Pt $4f_{5/2}$	Co $2p_{3/2}$	Co $2p_{1/2}$
$Pt_{50}Co_{50}$	71.58	74.88	780.78	796.68
$Pt_{34}Co_{66}$	71.48	74.88	780.38	797.48
$Pt_{21}Co_{79}$	71.58	74.88	780.88	796.78
$Pt_{16}Co_{84}$	71.48	74.78	780.68	796.38

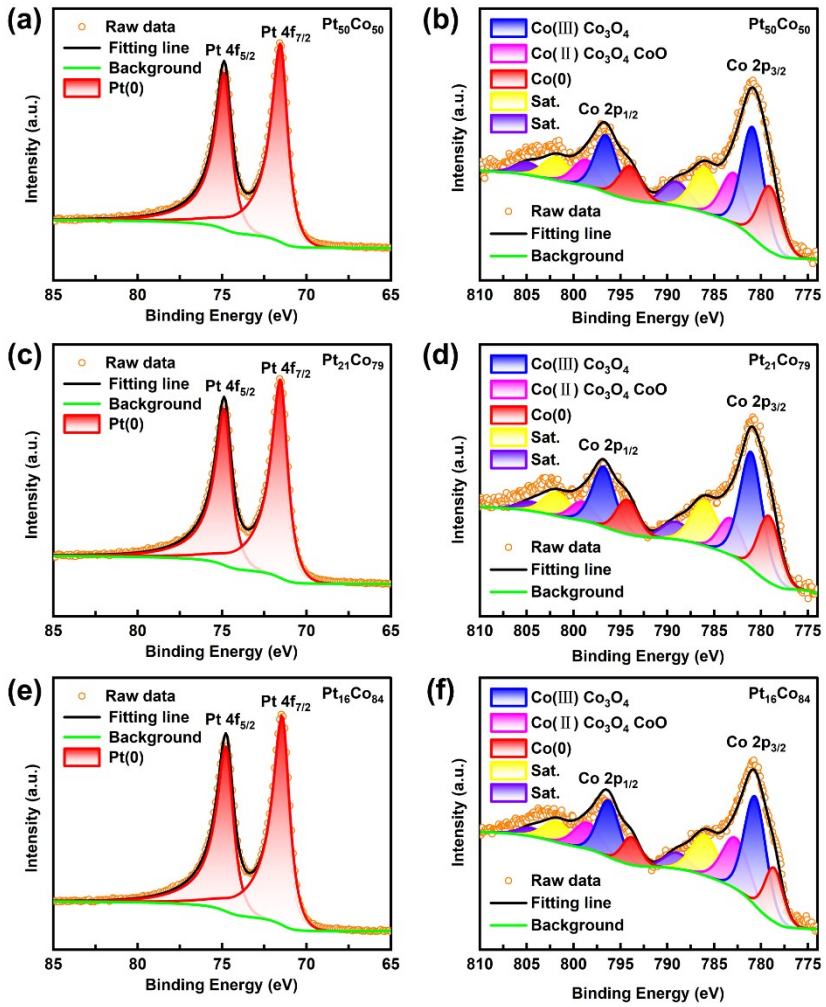

Fig. S4. High resolution XPS spectra of as-deposited (a, b) $Pt_{50}Co_{50}$, (c, d) $Pt_{21}Co_{79}$, and (e, f) $Pt_{16}Co_{84}$ films.

Table S2. The separate fitting results of the XPS peaks of as-deposited PtCo films in Fig. S4, Fig. 8a, and Fig. 8b.

Peaks	Binding energy (eV)			
	$Pt_{50}Co_{50}$	$Pt_{34}Co_{66}$	$Pt_{21}Co_{79}$	$Pt_{16}Co_{84}$
Pt $4f_{7/2}$	71.58	71.48	71.58	71.48
Pt $4f_{5/2}$	74.88	74.88	74.88	74.78
Co (0) $2p_{3/2}$	779.18	778.28	779.28	778.78
Co (0) $2p_{1/2}$	794.08	792.98	794.38	793.88
Co (III) $2p_{3/2}$	780.98	779.98	781.18	780.78
Co (III) $2p_{1/2}$	796.68	795.28	796.88	796.38
Co (II) $2p_{3/2}$	783.08	781.18	783.38	782.98
Co (II) $2p_{1/2}$	798.78	797.88	799.18	798.68
Co (III) $2p_{3/2}$ Sat.	786.08	786.08	786.08	786.18
Co (III) $2p_{1/2}$ Sat.	801.98	801.88	801.98	801.88
Co (II) $2p_{3/2}$ Sat.	789.18	789.78	789.18	789.08
Co (II) $2p_{1/2}$ Sat.	805.08	805.08	804.78	804.78

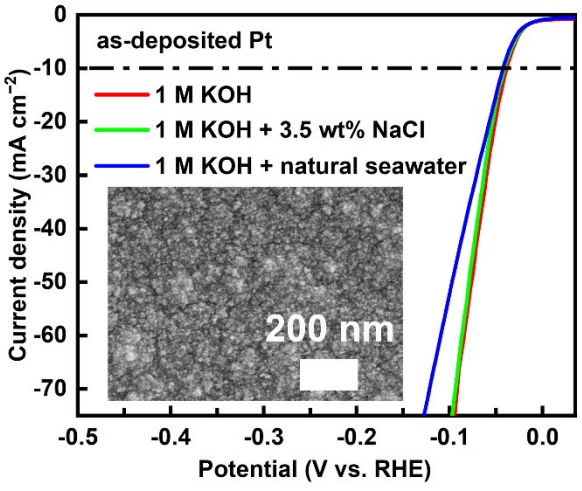

Fig. S5. LSV curves of as-deposited Pt films (the insert is SEM image).

Table S3. The HER performance of $Pt_{50}Co_{50}$, $Pt_{34}Co_{66}$, $Pt_{21}Co_{79}$, $Pt_{16}Co_{84}$, commercial Pt/C, and Pt in different electrolytes.

Electrolytes	Catalysts	Overpotential (mV vs. RHE)			Tafel slope (mV dec^{-1})
		@−10 mA cm^{-2}	@−50 mA cm^{-2}	@−70 mA cm^{-2}	
1M KOH	$Pt_{50}Co_{50}$	39	80	95	28
	$Pt_{34}Co_{66}$	35	63	75	24
	$Pt_{21}Co_{79}$	48	110	132	37
	$Pt_{16}Co_{84}$	55	124	147	49
	Pt/C	41	123	159	35
	Pt	39	77	92	-
1M KOH + 3.5 wt% NaCl	$Pt_{50}Co_{50}$	40	73	84	25
	$Pt_{34}Co_{66}$	33	63	76	22
	$Pt_{21}Co_{79}$	46	86	99	31
	$Pt_{16}Co_{84}$	45	111	133	36
	Pt/C	51	184	242	44
	Pt	41	79	94	-
1M KOH + natural seawater	$Pt_{50}Co_{50}$	35	71	83	39
	$Pt_{34}Co_{66}$	30	76	93	35
	$Pt_{21}Co_{79}$	35	79	95	38
	$Pt_{16}Co_{84}$	38	78	91	41
	Pt/C	50	221	299	88
	Pt	43	97	122	-

Table S4. EIS spectrum fitting data of $Pt_{50}Co_{50}$, $Pt_{34}Co_{66}$, $Pt_{21}Co_{79}$, $Pt_{16}Co_{84}$, and commercial Pt/C in different electrolytes.

Electrolytes	Catalysts	R_s (Ω)	R_{ct} (Ω)	W (Ω)
1M KOH	$Pt_{50}Co_{50}$	3.26	0.30	1.71
	$Pt_{34}Co_{66}$	3.68	0.29	1.52
	$Pt_{21}Co_{79}$	3.35	0.25	2.43
	$Pt_{16}Co_{84}$	3.03	0.25	3.08
	Pt/C	5.26	0.28	11.50
1M KOH + 3.5 wt% NaCl	$Pt_{50}Co_{50}$	3.12	0.18	1.38
	$Pt_{34}Co_{66}$	3.15	0.12	1.47
	$Pt_{21}Co_{79}$	3.03	0.16	1.95
	$Pt_{16}Co_{84}$	3.05	0.14	1.43
	Pt/C	4.56	0.37	11.85
1M KOH + natural seawater	$Pt_{50}Co_{50}$	2.91	0.30	1.91
	$Pt_{34}Co_{66}$	2.97	0.25	2.15
	$Pt_{21}Co_{79}$	3.10	0.39	2.51
	$Pt_{16}Co_{84}$	2.88	0.21	2.20
	Pt/C	5.64	0.21	8.09

Table S5. C_{dl} values, ECSA, and RF of $Pt_{50}Co_{50}$, $Pt_{34}Co_{66}$, $Pt_{21}Co_{79}$, $Pt_{16}Co_{84}$, and commercial Pt/C obtained in 1 M KOH + 3.5 wt% NaCl.

Catalysts	C_{dl} (mF)	ECSA (cm^2)	RF
$Pt_{50}Co_{50}$	1.89	47.13	188.50
$Pt_{34}Co_{66}$	3.48	86.94	347.75
$Pt_{21}Co_{79}$	2.53	63.19	252.75
$Pt_{16}Co_{84}$	2.45	61.19	244.75
Pt/C	1.88	46.88	187.50

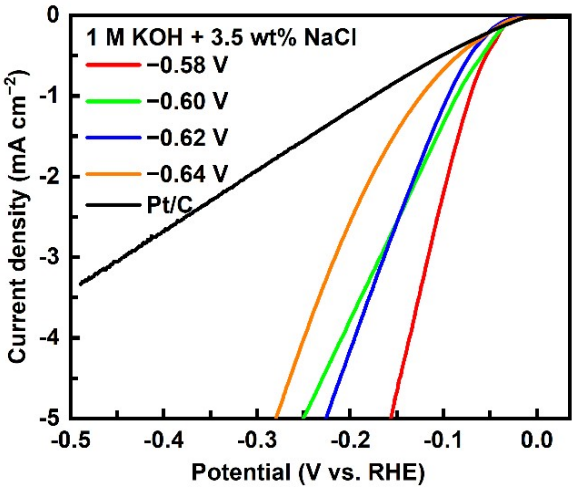

Fig. S6. LSV curves normalized by ECSA.

Table S6. The composition of $Pt_{34}Co_{66}$ (the as-prepared state and after the long-term aging stability test in 1M KOH + natural seawater) and electrolyte (1M KOH + natural seawater after the long-term aging stability test) determined by ICP-MS.

Sample	Element (at.%)			
	Pt	Co	Mg	Ca
$Pt_{34}Co_{66}$ at the as-prepared state	33.85	66.15	-	-
$Pt_{34}Co_{66}$ after long aging test	54.49	32.87	2.88	9.76
electrolyte	0.01	0.01	46.14	53.84

Chlorine corrosion mechanism of seawater HER

As for the electrocatalytic process taking place in alkaline simulated seawater (1 M KOH + 3.5 wt% NaCl) and alkaline natural seawater (1 M KOH + natural seawater), the aggressive chloride anions can form metal chlorides/hydroxides to corrode catalysts and substrates through the following mechanisms [S6, S7]:

Adsorption of Cl^- by surface polarization:

$$M + Cl^- \rightarrow MCl_{ads} - e^- \quad \text{(S11)}$$

Dissolution by further coordination:

$$MCl_{ads} + Cl^- \rightarrow MCl_x + e^- \quad \text{(S12)}$$

Conversion from chloride to hydroxide:

$$MCl_x + OH^- \rightarrow M(OH)_x + Cl^- \quad \text{(S13)}$$

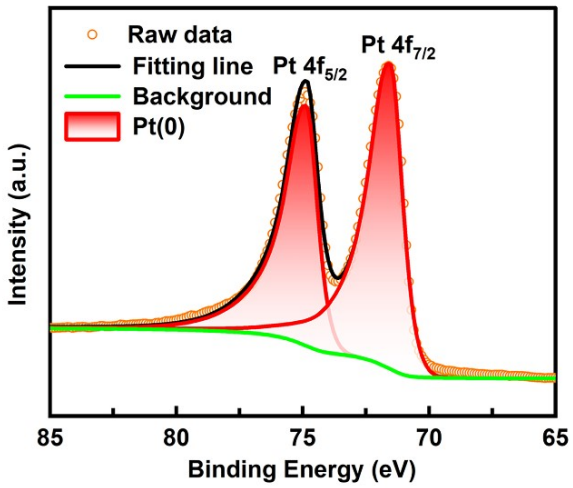

Fig. S7. High resolution XPS spectra of Pt 4f peaks of Pt deposited.

References

S1. Y. Chen, J. Zhang, J. Sort, E. Pellicer and R. Guan, International Journal of Hydrogen Energy, 2024, 59, 625-634.

S2. I. H. Cardona, E. Ortega, L. V. Gómez and V. P. Herranz, International Journal of Hydrogen Energy, 2012, 37, 2147-2156.

S3. S. Anwar, F. Khan, Y. Zhang and A. Djire, International Journal of Hydrogen Energy, 2021, 46, 32284-32317.

S4. Z. Zhou, Z. Pei, L. Wei, S. Zhao, X. Jian and Y. Chen, Energy & Environmental Science, 2020, 13, 3185-3206.

S5. E. Cossar, M. S. E. Houache, Z. Zhang and E. A. Baranova, Journal of Electroanalytical Chemistry, 2020, 870.

S6. X. Q. Zhang, Y. X. Xiao, G. Tian, X. Yang, Y. Dong, F. Zhang and X. Y. Yang, Chemistry, 2023, 29, e202202811.

S7. Y. Kuang, M. J. Kenney, Y. T. Meng, W. H. Hung, Y. J. Liu, J. E. Huang, R. Prasanna, P. S. Li, Y. P. Li, L. Wang, M. C. Lin, M. D. McGehee, X. M. Sun and H. J. Dai, Proceedings of the National Academy of Sciences of the United States of America, 2019, 116, 6624-6629.